Observation of Magnetized Soliton Remnants in the Wake of Intense Laser Pulse Propagation through Plasmas

L. Romagnani,[1,2] A. Bigongiari,[1,*] S. Kar,[1] S. V. Bulanov,[3] C. A. Cecchetti,[1,7] T. Zh. Esirkepov,[3] M. Galimberti,[4] R. Jung,[5] T. V. Liseykina,[6,†] A. Macchi,[7,8] J. Osterholz,[5] F. Pegoraro,[8] O. Willi,[5] and M. Borghesi[1]

[1]*Centre for Plasma Physics, School of Mathematics and Physics, The Queen's University of Belfast, Belfast BT7 1NN, United Kingdom*
[2]*LULI, École Polytechnique, CNRS, CEA, UPMC, route de Saclay, 91128 Palaiseau, France*
[3]*APRC, JAEA, Kizugawa, Kyoto 619-0215, Japan*
[4]*Central Laser Facility, Rutherford Appleton Laboratory, Chilton, United Kingdom*
[5]*Institut für Laser-und Plasmaphysik, Heinrich-Heine-Universität, Düsseldorf, Germany*
[6]*Max-Planck-Institut für Kernphysik, Heidelberg, Germany*
[7]*Istituto Nazionale di Ottica, CNR, Pisa, Italy*
[8]*Dipartimento di Fisica "E. Fermi," Università di Pisa, Pisa, Italy*

(Received 15 January 2010; published 19 October 2010)

Slowly evolving, regularly spaced patterns have been observed in proton projection images of plasma channels drilled by intense ($\gtrsim 10^{19}$ W cm^{-2}) short (~ 1 ps) laser pulses propagating in an ionized gas jet. The nature and geometry of the electromagnetic fields generating such patterns have been inferred by simulating the laser-plasma interaction and the following plasma evolution with a two-dimensional particle-in-cell code and the probe proton deflections by particle tracing. The analysis suggests the formation of rows of magnetized soliton remnants, with a quasistatic magnetic field associated with vortexlike electron currents resembling those of magnetic vortices.

DOI: 10.1103/PhysRevLett.105.175002 PACS numbers: 52.35.Sb, 52.38.Fz, 52.65.Rr, 52.70.Nc

The generation of coherent and ordered structures is one of the most prominent features in the dynamics of nonlinear many-body systems [1]. Theoretical and experimental studies have shown that plasmas interacting with laser pulses at relativistic intensities provide uniquely favorable conditions to investigate a broad class of nonlinear phenomena, the most known examples being arguably stimulated Raman and Brillouin scattering, laser filamentation and self-focusing, or the excitation of large amplitude wake plasma waves (see [2] and references therein). A different but not unrelated class of phenomena which has more recently attracted a great deal of attention includes the generation of organized nonlinear entities such as the so-called electromagnetic (EM) solitons [3–5] and electron vortices [6,7].

EM solitons have been extensively investigated both numerically [3] and in the frame of analytical models [4], and their macroscopic remnants [postsolitons (PSs)] have been experimentally observed to develop following the interaction of an intense laser pulse with a rarefied plasma [5]. Rows of electron vortices [6] and solitary magnetic dipole vortices (MDVs) [7] have been predicted to form in the trail of an intense laser pulse propagating in an underdense plasma. Besides being *per se* relevant as a benchmark for nonlinear plasma theoretical models, the experimental investigation of these phenomena might also have practical implications, as such nonlinear entities may contain a sizable fraction of the initial laser pulse energy [3–5] or be the signature of the development of plasma instabilities [6].

In this Letter we present the experimental observation, employing proton projection imaging (PPI) [8], of slowly evolving, localized EM structures, generated following the interaction at relativistic intensities of a picosecond laser pulse with an underdense plasma. These structures initially appear as a quasiperiodical pattern aligned along the low-density channel drilled by the laser pulse, and evolve on a time scale much longer than the pulse duration, remaining visible for more than 100 ps after the interaction. Simulations of the laser-driven plasma evolution carried out with a two-dimensional (2D) particle-in-cell (PIC) code show the development of EM solitons and their evolution into PSs inside laser-generated plasma channels [9]. Most noticeably the simulations indicate that, besides exhibiting properties typical of solitons (e.g., trapping of EM radiation in their inside and spatial localization consistent with the laser-pulse-depletion generation mechanism), these structures are also accompanied by vortexlike electron currents and quasistatic magnetic field patterns similar to those of MDVs. Extrapolating the results from 2D PIC simulations to the three-dimensional (3D) space, we can infer that in 3D the quasistatic magnetic field would assume a toroidal configuration (see also [3,7]). Particle tracing (PT) simulations [8] of the probe proton deflections show that such a 3D field distribution produces synthetic proton images consistent with the experimental observation.

The experiment was carried out at the Rutherford Appleton Laboratory (RAL), employing the VULCAN Nd-glass laser system operating in the chirped pulse

amplification (CPA) mode. A first laser pulse (1.054 μm wavelength, 1.2 ps duration, and delivering ~30 J energy on target in linear polarization, hereafter named CPA_1) was focused at intensities $\gtrsim 10^{19}$ W cm^{-2} onto a supersonic helium (He) jet (2 mm aperture diameter nozzle driven at 50 bar pressure). The main pulse was always preceded by a pedestal (~ 300 ps duration and $\sim 10^6$ contrast ratio) capable of preionizing the interaction region. The electron density profile (linearly ramping along the laser axis up to its peak value $\sim 1.5 \times 10^{20}$ cm^{-3} over a distance of ~400 μm and remaining constant after that, see also [10]) was diagnosed by *in situ* frequency-doubled optical interferometry with picosecond time resolution. Comparison of the electron density profile with a separate characterization of the neutral gas density in the gas jet [10] indicates full preionization of the gas.

The EM fields generated in the He plasma in the trail of the CPA_1 laser pulse were diagnosed employing a laser-driven transverse proton probe, arranged in a point projection geometry with single-shot temporal multiframe capabilities [8]. The proton beam was accelerated by focusing a second laser pulse (CPA_2) (with similar parameters to CPA_1) onto a thin metal foil (typically a 10 μm thick Au foil, proton target) and it was detected employing a multilayer stack of radiochromic films (RCFs). The distance of the proton target from the CPA_1 propagation axis was $l \sim 3$ mm, and from the RCF pack it was $L \sim 3$ cm, giving a projection magnification $M \simeq L/l \sim 10$. Spatial and temporal resolutions of a few μm and of a few ps, respectively, were achieved.

Typical PPI experimental data are shown in Fig. 1. In the images, regions of a darker (lighter) color compared to the background proton signal correspond to regions of accumulation (depletion) of the probe protons, and for our experimental conditions the proton density variations reflect the EM field gradients in the probed plasma. The laser pulse, linearly polarized in the z direction (i.e., along the normal to the page, z being the symmetry axis of the proton beam), is impinging from the left and by the earlier probing time $t \sim 3.5$ ps [1(a)] it has already exited the field of view to the right-hand side. In the proton images the channel drilled by the CPA_1 laser pulse into the ionized He jet is displayed as a lighter color region along x delimited by two dark lines [1(a)]. An additional dark line is visible near the channel axis on the left-hand side of the images. Longitudinal (i.e., reflecting a dependence of the deflecting fields on x) modulations first appear in the channel at probing times $t \gtrsim 5$ ps [1(b)], and later they evolve into a row of localized bubblelike structures aligned along the plasma channel and particularly evident on the right-hand side of the image 1(c). The localized structures slowly expand, remaining visible until the latest observation times ($t \gtrsim 140$ ps) [Fig. 2(a)], when they have evolved into a cloud of irregularly distributed bubbles. Whenever the plasma channel has split into secondary filaments, bubble structures are also observed inside some of the filaments [2(b)].

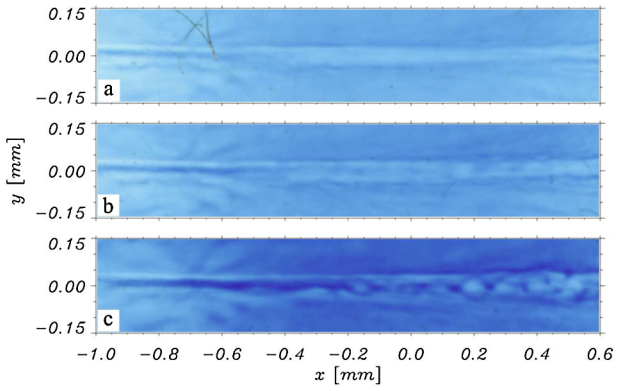

FIG. 1 (color online). Typical PPI data (acquired in a single laser shot). The probing times, relative to the arrival of the peak of the interaction pulse at $x = y = 0$, are (a) $t = 3.5$ ps, (b) $t = 7$ ps, and (c) 17 ps [probe proton energies ~12 MeV (a), ~11 MeV (b) and ~8 MeV (c)].

In order to infer on the nature of the observed patterns, the interaction of the laser pulse with the He plasma and the following plasma evolution were modeled with 2D PIC simulations [9]. The simulations were performed in a range of plasma densities and laser pulse parameters close to the experimental ones. In the following, lengths are in units of the laser wavelength λ, times in units of the laser period $T_L = \lambda/c = 2\pi/\omega$, densities in units of the critical density $n_c = m_e\omega^2/4\pi e^2$, and field amplitudes are expressed in terms of the dimensionless parameter $a = eE/m_e\omega c$ (see [9] for conversions to standard units). The largest grid employed in the simulations was a 7750×2400 mesh with a spatial resolution of $\lambda/10$, and the simulations were running up to a time $t = 1500T_L$. The plasma density was linearly ramping from zero at $x = 25\lambda$ to its peak value $n_e = 0.1n_c$ at $x = 425\lambda$, remaining constant after that. Ions with $Z/A = 1/2$ were assumed. The laser pulse (propagating along x) had a duration of $330T_L$, it was S polarized (electric field in the z direction, normal to the (x, y) simulation plane), and its field peak amplitude was $a = 2.7$.

In the simulation a low-density channel is ponderomotively bored into the plasma by the laser pulse, with the channel breaking into a number of secondary narrower channels in the higher background density region [9]. Following the initial evolution [9,10] and after the laser pulse has exited the simulation box, both the ion and

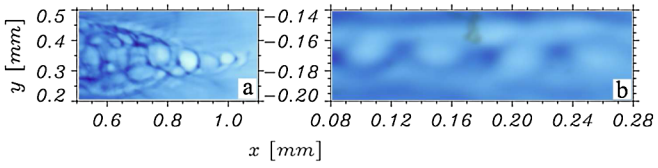

FIG. 2 (color online). (a) Detail of PPI data showing bubble structures at late times ($t \sim 140$ ps, probe proton energy ~8 MeV). (b) Detail of a secondary filament exhibiting a multiple bubble pattern ($t \sim 37$ ps, probe proton energy ~11 MeV).

electron densities are left with a depression on the channel axis while peaking at the channel edges, giving rise to a space-charge separation electric field, mainly in the y direction, E_y. At this stage ($t > 650T_L$) E_y has evolved into two ambipolar fronts on each side of the channel; i.e., it points outwards outside the channel and inwards inside it. An electron current is generated along the channel axis in the wake of the laser pulse (electrons flowing in the pulse propagation direction) and it is compensated by two current sheaths in the opposite direction along the channel edges. Such currents persist until the latest simulation times and produce a quasistatic magnetic field B_z, with $B_z < 0$ (i.e., entering the simulation plane) above the channel axis and $B_z > 0$ below it.

At even later times ($t > 750T_L$) the simulations show the onset of localized modulated patterns in the particle, current, and fields' distributions inside the main and secondary channels. A detail of the EM field distribution in a single localized structure is shown in Fig. 3. The frequency-resolved analysis of the fields reveals an oscillating EM field component (B_x, B_y, E_z) which has a frequency just below the plasma frequency of the surrounding plasma and is therefore trapped inside the structure [3(b) and 3(c)]. The current density forms an antisymmetric double loop, giving rise to a double lobe of quasistatic magnetic field B_z, with $B_z < 0$ above the channel axis and $B_z > 0$ below it [3(d)]. We stress here that this is a constant field, associated with a stationary electron current, differently from the oscillating field observed in other works [3] and also here. The combined effect of the magnetic pressure associated with the static B_z component and of the radiation pressure associated with the oscillating fields drills a density depression in correspondence with each localized structure. The resulting space-charge separation gives rise to a quasistatic electric field (E_x, E_y) in the radial direction from each structure center [3(a)]. Such field is less pronounced near the channel axis (due to the fact that the plasma density is lower here), and at the latest times ($t > 875T_L$) it tends to overlap with the ambipolar field at the channel edges.

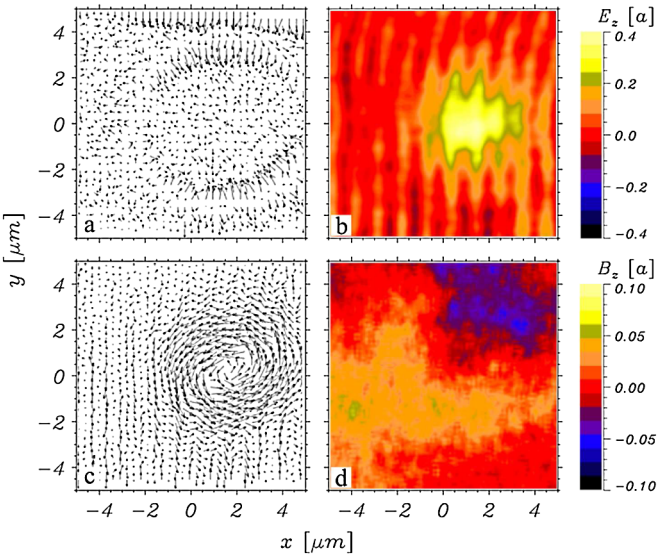

FIG. 3 (color online). Details of the fields' distribution in a single PS from PIC simulations. (a) Quasistatic electric field (E_x, E_y) at $t = 875T_L$, (b) oscillating electric field E_z, (c) oscillating magnetic field (B_x, B_y), and (d) quasistatic magnetic field B_z at $t = 800T_L$.

It should be noted here that the presence of a trapped oscillating field is typical of EM solitons and PSs, while the current and quasistatic magnetic field distributions resemble those of MDVs. As these features coexist and the static and oscillating fields are of similar strength, it is difficult to identify the observed structures with either solitons or vortices. However, their position in the plasma channels provides a hint of the mechanism leading to their formation and hence of their primary nature. The localization of the structures towards the end of the channels (both in the experiment and PIC simulations) is qualitatively consistent with estimations of the laser-pulse-depletion length ($l_{\mathrm{depl}} \sim cT_L(n_c/n_e) \sim$ mm range) [3], indicating that frequency downshift of the laser pulse and the consequent trapping of EM radiation is likely to be the relevant generation mechanism [3,4]. Hence the observed structures should be regarded as PSs. A likely scenario is that the electron currents readjust according to the density distribution associated with the preformed soliton structure, therefore giving rise to the vortexlike pattern. As these currents will always be present in the wake of a laser pulse propagating in an underdense plasma, a static magnetic field could be an unavoidable feature of laser-excited solitons.

To verify that the field distributions observed in the 2D PIC simulation, extrapolated to a 3D geometry, may produce the observed proton images, PT simulations [8] have been carried out. In PTs the deflections of test protons crossing a given 3D EM field distribution are numerically computed and the particle density in the proton detector is calculated. Only static fields have been considered, as for our experimental conditions the contribution of the oscillating components to the proton deflection is canceled out by integration along the particle trajectories. The input 3D field distribution is extrapolated from the 2D PIC outputs by assuming an azimuthal symmetry around the channel axis, and a reference frame with cylindrical coordinates (ρ, ϕ, x) (x being the channel axis) is considered. The electric field is chosen to be oriented along the radial $\hat{\rho}$ direction and the magnetic field to form closed loops in the azimuthal $\hat{\phi}$ direction.

We first simulated the deflections given by the fields associated with the plasma channel before the longitudinal modulations appear. In the simulation the electric field is taken of the form $E_\rho = f_-(\rho) + f_+(\rho)$, with $f_\pm(\rho) = 2.33E_0[(\rho \pm \alpha)/\beta]\exp\{-[(\rho \pm \alpha)/\beta]^2\}$, and the magnetic field of the form $B_\phi = 2.33B_0(\rho/\gamma) \times \exp[-(\rho/\gamma)^2]$, where the numerical factor 2.33 is chosen in order for E_0 and B_0 to represent the peak fields' amplitudes. The parameters α, β, and γ can be related to the

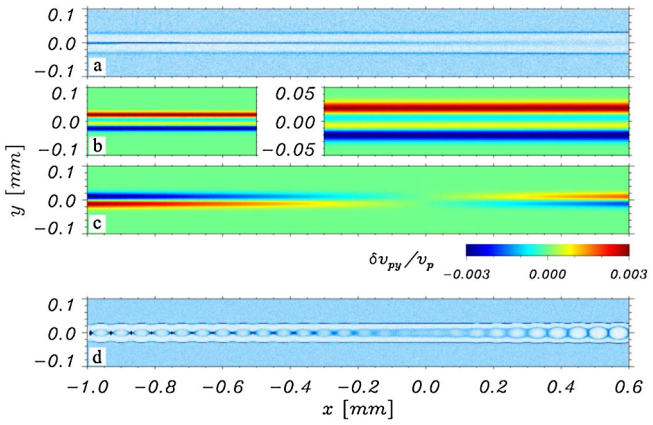

FIG. 4 (color online). Particle tracing simulations. (a) Simulated proton image and (b),(c) maps of the proton deflection $\delta\theta \sim \delta v_{py}/v_p$ arising from (b) the **E** field alone (y scale enlarged for $x > -0.5$ mm to highlight the E_y focusing effect inside the channel) and from (c) the **B** field alone for the unmodulated channel. (d) Simulated proton image for the modulated channel.

spatial characteristics of the PPI image of the channel, yielding $\alpha \simeq \gamma \simeq$ (15–20) μm and $\beta \simeq$ (5–10) μm. The PPI data were best reproduced for $E_0 \simeq (1\text{–}2) \times 10^9$ V m^{-1} and $B_0 \simeq$ (150–300) T [Fig. 4(a)], in fair agreement with the values obtained from the PIC simulations. Inspection of the PT results clarifies how the experimental proton images form. The ambipolar E_y field tends to pile up the protons on the channel axis and at the channel edges [see deflection map 4(b)]. The $v_{px}B_z$ component of the $\mathbf{v_p} \times \mathbf{B}$ ($\mathbf{v_p}$ being the proton velocity, with v_{px} mainly arising from the proton beam divergence) force tends to focus the protons on the axis for $x < 0$ (where $v_{px} < 0$, while $B_z < 0$ for $y > 0$ and $B_z > 0$ for $y < 0$), and at the channel edges for $x > 0$ (where $v_{px} > 0$) [4(c)]. Hence E_y gives rise to the dark lines delimiting the channel and contributes to the central dark line visible for $x < 0$. B_z contributes to the central dark line for $x < 0$, while for $x > 0$ it cancels the piling up on the channel axis given by E_y and contributes to the external dark lines.

We next introduce a modulation [described by a $\sin^2(2\pi x/l)$ weight function, where $l \simeq 60$ μm] of B_ϕ along the x direction. Such a field distribution describes a row of tori and represents the simplest possible extrapolation to a 3D geometry of the magnetic field associated with the vortexlike patterns observed in the 2D PIC simulations. The resulting simulated proton image [Fig. 4(d)] is in qualitative agreement with the experimental ones [Figs. 1(c) and 2]. The PT also indicates that the proton deflection in the y direction arises from the same effects described above, with additional longitudinal modulations in the proton density introduced by the B_ϕ dependence on x. We stress here that the presence of a modulated magnetic field, introduced for consistency with the 2D PIC simulations, is critical in order to reproduce the experimental data and that the proton deflection induced by the electric field alone cannot explain the experimental results.

In conclusion, we have shown that stable modulated patterns observed via PPI inside laser-plasma channels can be identified with the late time remnants of EM solitons observed in PIC simulations. PIC simulations also reveal the simultaneous presence of a quasistatic magnetic field associated with a vortexlike current distribution, and PT simulations evidence that such a magnetic field is essential for their experimental detection. The peculiar features of these structures, such as their magnetic nature, their organization into periodical patterns, and their detailed 3D topology, should be stimulating for further theoretical and numerical investigations.

We acknowledge the support of the RAL/CLF staff. This work has been supported by EPSRC Grants No. EP/E035728/1 (LIBRA consortium) and No. EP/C003586/1, by British-Council-MURST-CRUI, ESF-COST, TR18, and GRK1203 networks. Part of the simulations were performed at CINECA (Bologna, Italy) sponsored by CNR/INFM.

*Present address: CEA/DSM/IRAMIS/LSI, École Polytechnique, 91128 Palaiseau, France, and LULI, Université Paris VI, 3 rue Galilée, 94200 Ivry-sur-Seine, France.

†Present address: Institut für Physik, Universität Rostock, Rostock, Germany.

[1] T. Dauxois and M. Peyrard, *Physics of Solitons* (Cambridge University Press, Cambridge, England, 2006).
[2] G. A. Morou *et al.*, Rev. Mod. Phys. **78**, 309 (2006).
[3] S. V. Bulanov *et al.*, Phys. Fluids B **4**, 1935 (1992); S. V. Bulanov *et al.*, Phys. Rev. Lett. **82**, 3440 (1999); N. M. Naumova *et al.*, Phys. Rev. Lett. **87**, 185004 (2001); T. Esirkepov *et al.*, Phys. Rev. Lett. **89**, 275002 (2002); T. Esirkepov *et al.*, Phys. Rev. Lett. **92**, 255001 (2004).
[4] V. A. Kozlov *et al.*, Sov. Phys. JETP **49**, 75 (1979); P. K. Kaw, A. Sen, and T. Katsouleas, Phys. Rev. Lett. **68**, 3172 (1992); M. Lontano *et al.*, Phys. Plasmas **10**, 639 (2003).
[5] M. Borghesi *et al.*, Phys. Rev. Lett. **88**, 135002 (2002).
[6] S. V. Bulanov *et al.*, Phys. Rev. Lett. **76**, 3562 (1996); F. Califano, F. Pegoraro, and S. V. Bulanov, Phys. Rev. Lett. **84**, 3602 (2000); A. G. Zhidkov *et al.*, Phys. Rev. E **76**, 016401 (2007).
[7] N. M. Naumova *et al.*, Phys. Plasmas **8**, 4149 (2001); T. Nakamura and K. Mima, Phys. Rev. Lett. **100**, 205006 (2008).
[8] M. Borghesi *et al.*, Appl. Phys. Lett. **82**, 1529 (2003); A. J. Mackinnon *et al.*, Rev. Sci. Instrum. **75**, 3531 (2004).
[9] A. Macchi *et al.*, Plasma Phys. Controlled Fusion **49**, B71 (2007).
[10] S. Kar *et al.*, New J. Phys. **9**, 402 (2007).